Appl Phys B (2009) 95: 513–518
DOI 10.1007/s00340-009-3497-9

Applied Physics B
Lasers and Optics

Characteristics of holographic scattering and its application in determining kinetic parameters in PQ-PMMA photopolymer

H. Liu · D. Yu · Y. Jiang · X. Sun

Received: 28 November 2008 / Revised version: 2 February 2009 / Published online: 3 April 2009
© Springer-Verlag 2009

Abstract This paper characterizes holographic scattering and demonstrates its application in determining the kinetic parameters in materials with high transmittance and strong holographic scattering like phenanthrenequinone doped poly (methyl methacrylate) (PQ-PMMA). We define a polymerization rate parameter which can be determined by the temporal evolution of the scattering losses. Two basic kinetic parameters, quantum yield and molar-absorption coefficient, are obtained by nonlinear fitting the curve of the polymerization rate parameter as a function of the thickness, which are 1.9×10^{-6} mol/einstein and 2.1×10^{4} cm^2/mol for a wavelength of 532 nm respectively. These results improve the understanding of photochemical behaviors and allow us to describe the grating formation in the photopolymer reasonably.

PACS 42.70.Ln · 42.70.Jk · 42.40.Ht

1 Introduction

In recent years the interest in thick photopolymers for holographic information storage and optical data processing has increased [1–6]. One of the basic requirements for high-density storage is that the thickness of materials must be 500 μm or thicker [3]. Phenanthrenequinone (PQ) doped poly (methyl methacrylate) (PMMA) photopolymer is a potential holographic storage material due to its excellent ability to form thick mediums that exhibit high diffraction efficiency, neglectable shrinkage and good stability [4–12]. The applications of this material for high-density data storage and holographic optical elements have attracted much attention [8–12]. The photochemical reaction in this material is different from the typical chain polymerization in other polymers, such as acrylamide photopolymer. Under illumination the PQ molecules are photoexcited and bonded to the polymers. The refractive index modulation grows due to the photoattachment of PQ radicals to PMMA macromolecules. The unique photochemical reaction can provide a significant strategy for determining the kinetics parameters and optimizing fabrication of materials.

The determination of kinetic parameters is crucial for investigating the photochemical dynamics. Both the quantum yield and the molar-absorption coefficient of the photosensitizer are significant parameters which influence the photochemical behaviors of photopolymers [13]. Carretero et al. obtained the two parameters in acrylamide systems by analyzing the temporal growth of transmittance as a result of the bleaching of dye [13, 14]. This method, however, is not suitable for the PQ-PMMA photopolymer due to its high transmittance and strong holographic scattering. Holographic scattering is considered as a drawback because it limits the applicability of bulk materials. However it can advantageously be exploited in applications because of the properties of various material parameters [15, 16].

In this paper, we studied the observation of holographic scattering in PQ-PMMA photopolymer, and demonstrated its application in determining the kinetic parameters of photopolymers, for the first time to our knowledge. Reasonable parameters are obtained.

H. Liu · D. Yu · Y. Jiang · X. Sun (✉)
Department of Physics, Harbin Institute of Technology,
Harbin 150001, P.R. China
e-mail: xdsun@hit.edu.cn
Fax: +86-451-86414129

2 Materials and experimental setup

In our experiments, the samples were formed by poly (methyl methacrylate) (PMMA) host matrix and phenanthrenequinone (PQ) photosensitizer. The thermal initiator 2,2-azobis (2-methlpropionitrile) (AIBN) and PQ molecules were dissolved in a solvent methyl methacrylate (MMA) and mixed to form a uniform solution. The mixture was poured into a glass mold and solidified at 60°C for 120 h. After the thermal polymerization, the sample, with PQ's concentration of 0.1 M, was prepared.

A single beam experimental setup was used to investigate the holographic scattering in PQ-PMMA photopolymer, as shown in Fig. 1. A single collimated beam was incident to the surface of the sample. The incident beam was operated at a wavelength of 532 nm and *s*-polarization. The sample was placed on a computer-controlled motorized stage with a resolution of 0.0025°. The detectors D_1 and D_2 were used to detect the transmitted intensity and the fluctuation of the incident intensity, respectively.

3 Characteristics of holographic scattering

3.1 Parasitic grating formation

To get the details of holographic scattering in PQ-PMMA material, we investigate the parasitic grating formation in a collimated beam experiment firstly. Figure 2 shows the temporal evolution of the intensity distribution of far-field scattering light. The thickness of the sample is 2 mm. At the beginning, the scattered beams develop symmetrically around the incident beam. However, after 90 s exposure, an obvious scattered ring pattern appears in the left underside of the screen.

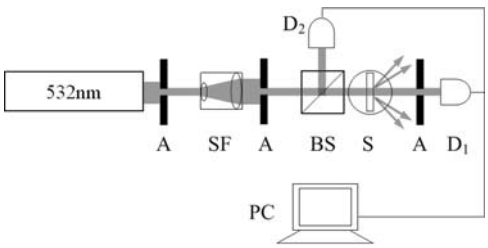

Fig. 1 Experimental setup: A: aperture, BS: beamsplitter, SF: spatial filter, S: sample, D_1, D_2: detectors, PC: data recorder

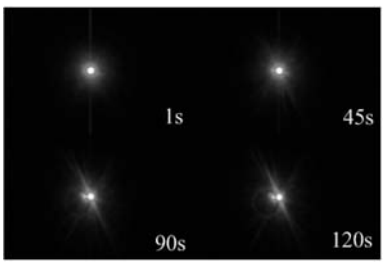

Fig. 2 Temporal evolution of intensity distribution of far-field scattering light

In this experimental setup, parasitic gratings are formed by the interference of the original incident beam with the scattered lights from the inhomogeneities of the sample and the reflected beams from the back surface. This scattered ring comes from the spatial distribution of scattering beams which are diffracted by parasitic gratings [17]. The diameter of this circle is related to the directions of both the scattered beams and the reflected beams from the back surface of the sample.

After recording parasitic gratings in the exposure spot, we rotate the sample by a motorized stage and probe the diffraction patterns using collimated 532 and 633 nm laser beam simultaneously. Two diffraction rings are observed on a screen placed behind the sample. The diameters of these rings as a function of the read-out angles are shown in Fig. 3. The phenomenon of two diffraction rings in polymer was first reported by Moran and Kaminow in 1973 [18] and was explained by the Ewald sphere construction [17]. The schematic explanation of two ring patterns in reciprocal space was shown in Fig. 3(b). The basic idea was the following [19, 20]: the refractive index changes by interference between the incident beam and scattering beam takes place on two spheres which are named the primary and conjugate sphere. The two spheres for recorded parasitic gratings intersected with the reading sphere. Diffraction of the read-out light occurred at intersected places, resulting in two cones which projected on the screen and produced two bright rings. The apex angle of the cones was given by the equation [17, 21, 22]

$$\xi = 2\arctan\left(\frac{\sin\theta_r}{\cos\theta_r \pm \lambda_p/\lambda_r}\right), \tag{1}$$

where θ_r is the read-out angle of incident beam within the medium. λ_r and λ_p are read-out and pump wavelength respectively. The positive and negative sign are assigned to the conjugate and primary sphere, respectively.

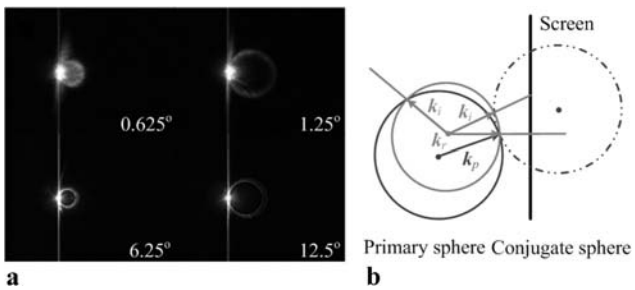

Fig. 3 (**a**) Two rings of diffraction patterns at different read-out angle for wavelengths of 532 and 633 nm. (**b**) Schematic explanation in terms of the Ewald sphere construction

By rotating the sample we measure the apex angle of the smaller ring as a function of the read-out angle at 532 and 633 nm, respectively. The results indicate an obvious linear relationship over the read-out angle range from −30 degree to 30 degree, as shown in Fig. 4. It is demonstrated that this phenomenon is ascribed to the holographic scattering.

3.2 Analysis of parasitic gratings

During exposure, the scattering field can be treated as the superposition of a larger number of plane waves, and each plane wave interferes with the incident beam, producing a plane grating. The parasitic grating may be treated as the sum of a larger number of weak plane gratings [23]. The contributions of weak plane gratings on the refractive index modulation of parasitic grating can be considered as a total impaction. Therefore the refractive index modulation of the parasitic grating can be described approximately by a plane grating. The scattering ratio is generally defined as the total scattering intensity outside the incident beam divided by the initial transmitted intensity [9].

$$S(t) = \left(1 - \frac{I_T(t)}{I_0}\right) \times 100\%, \tag{2}$$

where $I_T(t)$ is transmitted intensity at t time, I_0 is initial transmitted intensity. The scattering ratio can also be considered as the diffraction efficiency of parasitic gratings. According to the Kogelnik theory [24], we can obtain

$$\arcsin\left(\sqrt{S(t)}\right) \propto \Delta n(t), \tag{3}$$

where $\Delta n(t)$ is the refractive index modulation of parasitic gratings.

4 Application of holographic scattering in determining kinetic parameters

The holographic scattering method may be used to determine the quantum yield and the molar-absorption coefficient in PQ-PMMA photopolymer. In comparison with two-wave coupling, the holographic scattering can be achieved more easily due to the simple and steady experimental setup (only one beam, no sensitivity to vibrations). It is especially significant for long term experiments. Moreover, it reflects the real situation of optical data storage with a host of gratings recorded, whereas only one grating is created in two-wave coupling.

4.1 Photochemical mechanism

Firstly, we briefly analyzed the physical mechanism of photochemical reaction inside the sample. The primary photoattachment of PQ radicals to the PMMA macromolecules can be described as [4–10]

$$\mathrm{PQ} \xrightarrow{k_d} \mathrm{PQ}^{\bullet}, \tag{4}$$

$$\mathrm{PQ}^{\bullet} + \mathrm{HR} \xrightarrow{k_i} \mathrm{HPQ}^{\bullet} + \mathrm{R}^{\bullet}, \tag{5}$$

$$\mathrm{HPQ}^{\bullet} + \mathrm{R}^{\bullet} \xrightarrow{k_t} \mathrm{RQPH}, \tag{6}$$

where R represents the polymer matrix. k_d, k_i, and k_t are the rate constants of radical generation, initiation and termination respectively. Under uniform irradiance the spatial dependence of the diffusion coefficient of PQ molecules disappears [25]. Moreover, the residual PQ molecules in the dark region of parasitic gratings are photoexcited and bond to the PMMA matrix by the subsequent homogeneous illumination due to the low diffusion coefficient, 10^{-21} m^2/s [6]. Therefore the diffusion processes of the primary components can be prevented.

The primary molecule consumption is related to both the free radical generation and initiation reactions,

$$-\frac{\partial[\mathrm{PQ}](t)}{\partial t} = R_d + R_i, \tag{7}$$

where R_d is the rate of free radical generation, R_i is the rate of initiation reaction, and [PQ] is the concentration of PQ molecules. R_i is generally much greater than R_d, and therefore the rate of the initiation reaction can be written as $R_i = f k_d[\mathrm{PQ}]$ [26]. f presents the fraction of radicals reacted due to the cage effect only [26, 27]. Consequently the solution of (7) is given by

$$[\mathrm{PQ}](t) = [\mathrm{PQ}]_0 \exp(-f k_d t) = [\mathrm{PQ}]_0 \exp(-E/E_\tau), \tag{8}$$

where E is exposure energy, $E_\tau = I_0/f k_d = 1/\kappa$, κ is defined as the polymerization rate parameter. On the other hand, the initial rate of dye molecules is proportional to the incident intensity which can be given by $R_i = \Phi I_a/d$ [28]. The initial rate is considered as the primary polymerization rate due to the unique photochemical reaction [25, 28, 29]. Therefore the dependence of the primary polymerization rate of photochemical reaction on the intensity is linear. The growth evolution of corresponding polymer density can be represented as

$$[\mathrm{Polymer}](E) = [\mathrm{PQ}]_0\left[1 - \exp(-E/E_\tau)\right]. \tag{9}$$

The refractive index modulation is proportional to the density of primary components in any point [28]:

$$\Delta n(E) \propto [\mathrm{Polymer}](E) + [\mathrm{PQ}](E)\exp(i\phi), \tag{10}$$

where the phase ϕ corresponds to the relative phase difference between two offsetting gratings. Substituting (8) and

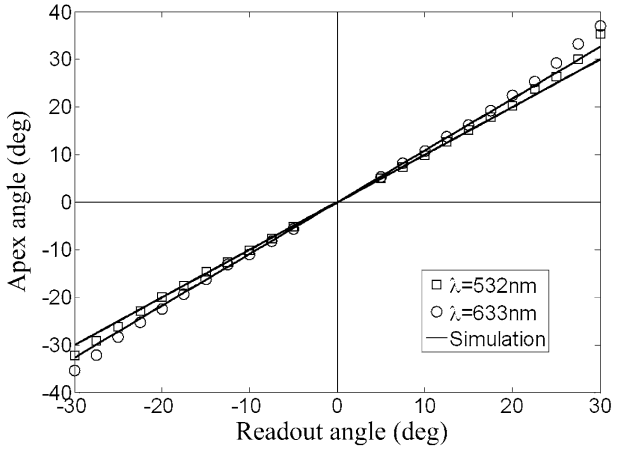

Fig. 4 The apex angle of conjugate sphere versus read-out angle for wavelengths of 532 and 633 nm, respectively. The *symbols* are experimental results and the *solid lines* are simulations of (1) for corresponding wavelength

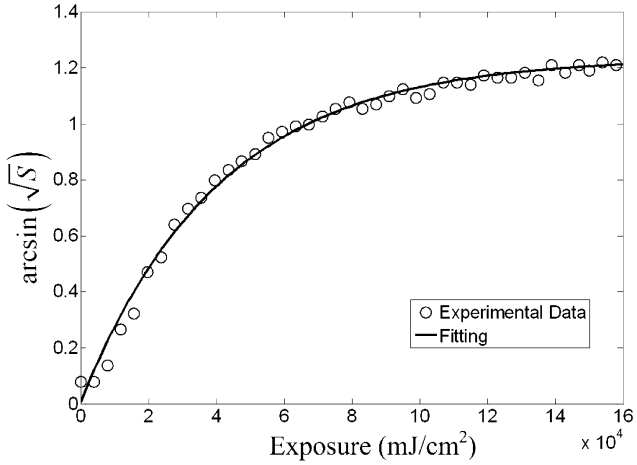

Fig. 5 Square root of the scattering ratio as a function of the exposure. The *symbols* are experimental data and the *solid line* is a fitting curve by using an exponential function. The thickness of the sample is 1.0 mm

(9) into (10), the refractive index modulation grows following an asymptotic curve,

$$\Delta n(E) = C_1 - C_2 \exp(-E/E_\tau), \tag{11}$$

with constants C_1, C_2.

According to (3), the refractive index modulation of parasitic grating can be described by (11). We measured the temporal evolution of the scattering ratio. The typical experimental curve of the square root of the scattering ratio, being a function of exposure energy, is shown in Fig. 5. The circles represent experimental data, and the solid line represents the fitting curve by the exponential function. The transmitted intensity detected by detector D_1 decreases with the exposure increasing until it reaches a steady minimum. The polymerization rate parameter, which is inversely proportional to the constant E_τ, was given as 2.5×10^{-5} cm^2 mW^{-1} s^{-1}.

4.2 Determination of kinetic parameters

Initiation mechanisms of free radicals formation generally involve the photochemical electron transfer reaction. The generation of monomer radicals is dependent on the quantity of free radicals formed per photon absorbed and the intensity used for recording. Thus the rate of the initiation reaction can be rewritten as [13, 28, 30]

$$R_i = \frac{\Phi I_a}{d}, \tag{12}$$

$$I_a = I_0[1 - T] = I_0\big[1 - T_f \exp\big(-\varepsilon d[\mathrm{PQ}]\big)\big], \tag{13}$$

where Φ is the quantum yield for the radical production, ε is the molar-absorption coefficient, d is the thickness of the sample, T is the transmittance defined as $I_T(t)/I_0$, and T_f is a parameter taking into account reflected light. Relating (12) and $R_i = f k_d[\mathrm{PQ}]$, we can obtain

$$f k_d[\mathrm{PQ}] = \frac{\Phi I_0}{d}\big[1 - T_f \exp\big(-\varepsilon d[\mathrm{PQ}]\big)\big]. \tag{14}$$

The relationship between the polymerization rate parameter and the thickness of the sample appears as follows by simplifying (14) at the initial time:

$$\kappa = \frac{\Phi}{d[\mathrm{PQ}]_0}\big[1 - T_f \exp\big(-\varepsilon d[\mathrm{PQ}]_0\big)\big]. \tag{15}$$

The quantum yield Φ and molar absorption coefficient ε can be obtained by nonlinear fitting the curve of polymerization rate parameter as a function of thickness.

Figure 6 shows the polymerization rate parameter κ as a function of the thickness of the sample. The solid curve represents the nonlinear fitting using (15). The kinetic parameters of the polymerization reaction are determined by the nonlinear fitting of this curve. The corresponding results for the quantum yield and molar absorption coefficient are shown in Table 1. For comparison, the parameters of other dyes in acrylamide photopolymer systems are included in Table 1. As can be seen, the kinetic parameters of PQ molecules are lower than the values of methylene blue (MB) and Azure-C (Ac) dyes, which is ascribed to the low absorbance of the sample at a wavelength of 532 nm [5, 13].

4.3 Results from transmittance measurements

To prove that our approach may lead to reasonable results, the parameters were calculated using another method. According to the relationship between the initial transmittance of sample and the molar absorption coefficient, at initial time

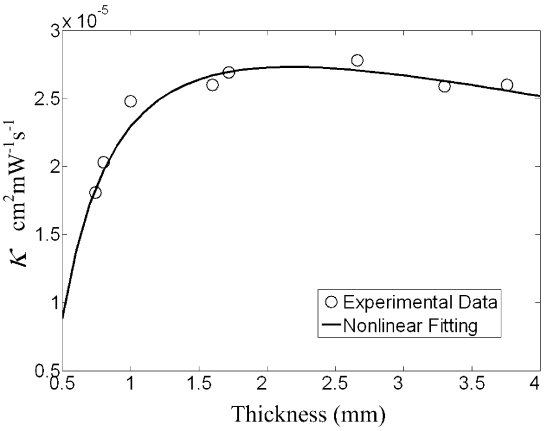

Fig. 6 Polymerization rate parameter versus thickness of the sample. The *symbols* are experimental data and the *solid line* is the nonlinear fitting curve

Table 1 Quantum yield Φ and molar absorption coefficient ε of the photosensitizer

Photosensitizer	ε (cm^2/mol)	Φ (mol/einstein)	λ (nm)
PQ[a]	2.1×10^4	1.9×10^{-6}	532
PQ[b]	1.3×10^4	2.7×10^{-6}	532
MB [13]	7.29×10^7	0.032	633
Ac [13]	5.88×10^7	0.050	633

[a]Parameters are obtained from the fitting curve of polymerization rate parameter versus thickness of sample

[b]Parameters are estimated values based on (16) and (17)

Table 2 Kinetic parameters from the transmittance measurements

Thickness (mm)	Transmittance (%)	ε (cm^2/mol)	Φ (mol/einstein)
0.8	85.2	2.0×10^4	1.1×10^{-6}
1.2	85.0	1.4×10^4	2.0×10^{-6}
2.7	78.5	0.9×10^4	3.5×10^{-6}
3.8	76.7	0.7×10^4	4.2×10^{-6}

we can obtain [28]

$$\varepsilon = \frac{-\log(T_0)}{d[\mathrm{PQ}]_0}, \tag{16}$$

where T_0 is the initial transmittance of the sample. At the same time the approximate representation of quantum yield can be represented as based on (14),

$$\Phi = \frac{f k_d [\mathrm{PQ}]_0 d}{I_0[1 - T_0]}. \tag{17}$$

To obtain these parameters, we measure the initial transmittance of the sample with different thickness. The corresponding values of these parameters are shown in Table 2. It is found that the average values of both the quantum yield, 2.7×10^{-6} mol/einstein, and the molar absorption coefficient, 1.3×10^4 cm^2/mol, are close to the fitting values in Table 1. Therefore the kinetic parameters obtained by holographic scattering are reasonable and acceptable.

5 Conclusions

A detailed study of holographic scattering in PQ-PMMA photopolymer is presented. We demonstrated holographic scattering as an efficient method to determine the kinetic parameters. The method is based on a certain assumption to describe the photochemical processes and it is suitable for measuring the materials with high transmittance. The quantum yield and the molar absorption coefficient are obtained for the first time in a PQ-PMMA system. They provide real kinetic parameters to describe the photochemical dynamics. The results enhance the understanding of photochemical behaviors and confirm the applicability of holographic scattering.

Acknowledgements The research has been financially supported by the Fundamental Research Foundation of the Commission of Science Technology and Industry for National Defense of China (Grant No. 2320060089).

References

1. P. Cheben, M.L. Calvo, Appl. Phys. Lett. **78**, 1490–1492 (2001)
2. E. Fernandez, C. Garcia, I. Pascual, M. Ortuno, S. Gallego, A. Belendez, Appl. Opt. **45**, 7661–7666 (2006)
3. H.J. Coufal, D. Psaltis, G.T. Sincerbox (eds.), *Holographic Data Storage* (Springer, New York, 2000)
4. G.J. Steckman, I. Solomatine, G. Zhou, D. Psaltis, Opt. Lett. **23**, 1310–1312 (1998)
5. S.H. Lin, K.Y. Hsu, W.Z. Chen, W.T. Whang, Opt. Lett. **25**, 451–453 (2000)
6. A.V. Veniaminov, Yu.N. Sedunov, Polym. Sci. Ser. A **38**, 56–63 (1996)
7. A.V. Veniaminov, E. Bartsch, J. Opt. A, Pure Appl. Opt. **4**, 387 (2002)
8. Popov, A. Novikov, K. Lapushka, I. Zyuzin, Y. Ponosov, Y. Ashcheulov, A.V. Veniaminov, J. Opt. A, Pure Appl. Opt. **2**, 494–499 (2000)
9. K.Y. Hsu, S.H. Lin, Opt. Eng. **42**(5), 1390–1396 (2003)
10. L.P. Krul, V. Matusevich, D. Hoff, Opt. Express **15**, 8543–8549 (2007)
11. V. Matusevich, A. Matusevich, R. Kowarschik, Yu.I. Matusevich, L.P. Krul, Opt. Express **16**, 1552–1558 (2008)
12. Y. Luo, P.J. Gelsinger, J.K. Barton, Opt. Lett. **33**, 566–568 (2008)
13. L. Carretero, S. Blaya, R. Mallavia, F. Madrigal, A. Beléndez, A. Fimia, Appl. Opt. **37**, 4496–4499 (1998)
14. S. Blaya, L. Carretero, R. Mallavia, F. Madrigal, A. Fimia, R.F. Madrigal, Appl. Opt. **38**, 955–962 (1999)
15. M.A. Ellabban, M. Fally, R.A. Rupp, Holographic scattering and its applications, in *Recent Research Developments in Applied Physics*, Part IV, June (2001)
16. M.A. Ellabban, G. Mandula, M. Fally, Appl. Phys. Lett. **78**, 844–846 (2001)

17. M.R.B. Forshaw, Appl. Opt. **13**, 2 (1974)
18. J.M. Moran, I.P. Kaminow, Appl. Opt. **12**, 1964 (1973)
19. M.A. Ellabban, M. Fally, M. Imlau, J. Appl. Phys. **96**, 6987–6993 (2004)
20. M. Fally, M.A. Ellabban, R.A. Rupp, Phys. Rev. B **61**, 15778–5784 (2000)
21. M.A. Ellabban, M. Fally, Appl. Phys. Lett. **87**, 151101 (2005)
22. R. Magnusson, T.K. Gaylord, Appl. Opt. **13**, 1545–1548 (1973)
23. J.A. Frantz, R.K. Kostuk, D.A. Waldman, J. Opt. Soc. Am. A **21**, 378–387 (2004)
24. H. Kogelnik, Bell System Tech. J **48**, 2909–2947 (1969)
25. V. Moreau, Y. Renotte, Y. Lion, Appl. Opt. **41**, 3427–3435 (1999)
26. J.V. Kelly, F.T. O'Neill, J.T. Sheridan, J. Opt. Soc. Am. B **22**, 407–416 (2005)
27. G. Odian, *Principle of Polymerization* (Wiley, New York, 1991)
28. J.H. Kwon, H.C. Hwang, K.C. Woo, J. Opt. Soc. Am. B **16**, 1651–1657 (1999)
29. S. Piazzolla, B.K. Jenkins, J. Opt. Soc. Am. B **16**, 1147–1157 (2000)
30. S. Blaya, L. Carretero, R.F. Madrigal, A. Fimia, Appl. Phys. B **74**, 243–251 (2002)